Manipulation of a Micro-Object Using Topological Hydrodynamic Tweezers

Peiran Yin,[1,2] Rui Li,[1,2,3] Zizhe Wang,[1,2] Shaochun Lin,[1,2] Tian Tian,[1,2] Liang Zhang,[1,2] Longhao Wu,[1,2] Jie Zhao,[1,2] Changkui Duan,[1,2] Pu Huang,[4,*] and Jiangfeng Du[1,2,3,†]

[1] *CAS Key Laboratory of Microscale Magnetic Resonance and Department of Modern Physics, University of Science and Technology of China, Hefei 230026, China*

[2] *Synergetic Innovation Center of Quantum Information and Quantum Physics, University of Science and Technology of China, Hefei 230026, China*

[3] *Hefei National Laboratory for Physical Sciences at the Microscale, University of Science and Technology of China, Hefei 230026, China*

[4] *National Laboratory of Solid State Microstructures and Department of Physics, Nanjing University, Nanjing 210093, China*

(Received 6 May 2019; revised manuscript received 8 August 2019; published 8 October 2019)

Manipulating microscale object plays a paramount role in a wide range of fundamental research efforts and applications. At the microscale, various methods have been developed in the past decades, including optical, electric, magnetic, aerodynamic, and acoustic methods. However, these noncontact forces are susceptible to external disturbance, and so finding a way to make microscale object manipulation immune to external perturbations is challenging and remains elusive. Here, we demonstrate a method based on a trapping mechanism to manipulate a microscale object in a gas flow at ambient conditions. We first show that the microdroplet is entrapped in a trapping ring constructed by a particular toroidal vortex. The vortex works as tweezers to control the position of the microdroplet. We then show that the microdroplet can be transported along the trapping ring. By virtue of the topological character of the gas flow, the transport path is able to bypass external strong perturbations automatically. We further demonstrate a topological transfer process of the microdroplet between two hydrodynamic tweezers. Our method provides an integrated toolbox to manipulate a microscale object, with an intrinsic mechanism that protects the target object from external disturbances.

DOI: 10.1103/PhysRevApplied.12.044017

I. INTRODUCTION

Manipulating a microscale object is always a challenging issue in various fundamental research efforts and applications. Because methods based on direct mechanical contact fail at the microscale, various noncontact methods have been developed in the past decades, including optical [1], electric [2], magnetic [3], aerodynamic [4], and acoustic [5] methods. These methods have found wide applications in physics [6,7], chemistry [8], biology [9,10], and information science [11,12]. However, because of the fragility of the noncontact force, the manipulation of a microscale object is often susceptible to external disturbance.

Topological phenomena have been observed in various physics systems recently, involving charge [13] and spin transport [14,15], optical photons [16–19], microwaves [20,21], mechanical vibrations [22], and acoustics [23]. One topological phenomenon's character is such that the global transport process is immune to local disturbance [24].

In fluid dynamics, the vorticity $\boldsymbol{\Omega}$ is a pseudovector field that describes the vortex field, and it is defined as the curl of the flow velocity $\boldsymbol{\upsilon}$, i.e., $\boldsymbol{\Omega} = \nabla \times \boldsymbol{\upsilon}$. For an incompressible fluid, vorticity has the special property that its field lines never cross. This indicates an important topological property that knotted or linked loops in the fluid remain knotted or linked even in the presence of viscosity or external local perturbations [25,26]. Besides fundamental interest, whether such topological properties have any practical application remains to be explored.

Here, we generate a particular toroidal vortex using a tapering micronozzle, which works as tweezers to manipulate the microdroplet at ambient conditions. In this trapping mechanism, the particle released in gas flow is entrapped in the vortex core under the action of Stokes drag force from the vortex flow and a restoring force in the gravity direction. By taking advantage of the nonlocal topological property of the vortex flow field, we further demonstrate the transport and transfer of the object in a controllable way that is intrinsically protected from external disturbance.

*hp@nju.edu.cn
†djf@ustc.edu.cn

II. CONCEPT OF THE HYDRODYNAMIC TWEEZERS

For a microparticle released in a nonuniform flow, determining the drag and lift forces arising from both inertia and unsteady effects at a low Reynolds number is a long-standing open question in fluid dynamics [27–29]. Intuitively, when a micro-object is released in a swirling fluid flow, it is predicted to spiral toward the equilibrium point close to the center of the vortex core. Actually, it is verified in our experiment that, at a low Reynolds number around 0.001, a heavy microparticle in the particular toroidal vortex is entrapped in a trapping ring spirally. We can manually pull the microparticle to transport along the ring.

Before building practical hydrodynamic tweezers, three issues need to be addressed. First, the size of the object to be trapped is dependent on the characteristic scale of fluid flow, and so it is possible, in principle, to realize the control of an arbitrarily small object. However, as the system scales down, the condition of continuous fluid would fail and the molecular behaviors would emerge. The typical value of the mean free path is tens of nanometers for a gas phase flow in a practical realization and subnanometer when a liquid phase fluid is used. The second issue is the fluctuation of the fluid field. As the fluid flows past an object, the object also exerts a back action onto the fluid. This effect is characterized by the Reynolds number (Re). When Re is large enough, turbulence occurs and the system becomes unstable. For micro-objects, however, the typical Re is usually small enough to avoid turbulence. The third issue is related to the viscosity. As a vortex in a nonideal fluid will eventually spread and damp out, a suitable external pump is necessary to maintain the main structure of the vortex.

The scheme of our hydrodynamic tweezers is shown in Fig. 1(a). The gas flows from a tapering micronozzle and generates a toroidal vortex downstream. A microscale particle set around the vortex tube feels a trapping force $\mathbf{F}_T$, which attracts the object toward the vortex center that forms a ring in the x-y plane. So such a particle can be trapped on the ring steadily with this hydrodynamic tweezers.

The generated flow field is symmetric around the z axis. So the flow patterns can be clearly demonstrated by the streamlines [31] in the y-z plane as shown in Fig. 1(b). The stream function is defined by

$$\Psi = \int_0^y v_z y \, dy, \tag{1}$$

where v_z is the magnitude of velocity of the gas flow in the z direction. The stream function is obtained by a numerical simulation of the flow field [32], which

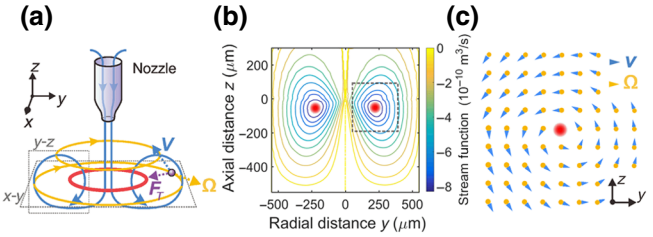

FIG. 1. Concept of the hydrodynamic tweezers. (a) Schematic plot of the system. Gas flow indicated as blue field lines comes from a micronozzle and generates a vorticity field $\mathbf{\Omega}$, indicated as yellow field lines. An object is indicated as a purple sphere, which spins with the vortex field. This object feels a trapping force $\mathbf{F}_T$, which pulls it toward the trapping ring shown as a red circle. The object can move along the ring and is stably trapped in the ring. (b) Streamlines of the fluid flow in the y-z plane. The red dot marks the trapping point. (c) Numerical simulation of the velocity and vorticity fields in the cross section shown as a dotted box in (b). They are indicated by blue arrows and yellow dots, respectively. The size of marks is proportional to the field strength and the region is about 100 by 100 μm. In the simulation, the nozzle diameter is 20 μm, and the maximum velocity at the nozzle outlet is 3.2 ms^{-1} (see Sec. I of the Supplemental Material [30]).

is described in detail in Sec. I of the Supplemental Material [30]. As indicated in Fig. 1(b), the vortex core is formed over one nozzle diameter length downstream. The flow around the vortex core can be approximately described as a forced vortex in the y-z plane with a vortex center at the vortex core. The angular velocity ω is around $2\pi \times 16$ Hz. The velocity and vorticity fields in the cross section shown as a dotted box in Fig. 1(b) are indicated by blue and yellow marks, respectively, in Fig. 1(c). The vorticity $\mathbf{\Omega}$ is invariant around the vortex center with $\Omega = 2\omega$. With the distance from vortex center no more than 50 μm, the maximum velocity deviation from the forced vortex model is within 20%.

For a particle released near the toroidal vortex at a low Reynolds number, it feels drag and lift forces from the flow [27–29]. With the main concern being about the trapping process near the vortex core, it is reasonable to approximately treat the flow in the vicinity of the vortex core in one cross section (i.e., the y-z plane) as a forced vortex. Then the trapping dynamics can be further studied analytically.

III. TRAPPING THEORY

The Reynolds number of the flow is $\mathrm{Re} = d\upsilon\rho/\mu$, where d is the diameter of the nozzle; υ is the magnitude of velocity of fluid flow; and ρ and μ are the fluid's density and viscosity coefficient, respectively. For the micronozzle in our scheme, Re is much less than 10, which is far from a turbulent condition. Similarly, the particle Reynolds number $\mathrm{Re}_p = a\upsilon_s\rho/\mu$ is around 0.001. Here, a is the radius of

the particle and υ_s is the magnitude of relative velocity of the particle and fluid measured on the streamline through the center of the particle (i.e., $\mathbf{v}_s = \mathbf{v}_p - \mathbf{v}$).

In our setup, a liquid microscale droplet is released in a gas flow at ambient conditions. So the buoyancy and the classical pressure gradient of the unperturbed flow can be ignored comparing with the Stokes drag force. The force analysis of the droplet in fluid flow is shown in Fig. 2(a). The gravity of the droplet is balanced by the diamagnetic force generated by an array of magnets (see Sec. II of the Supplemental Material [30] for more detail). Therefore, the droplet feels a restoring force $\mathbf{F}_m = -k\mathbf{z}$ in the z direction near the equilibrium position. In the limit of $1 \gg T_a^{1/2} \gg \mathrm{Re}_p$, where $T_a = a^2\omega\rho/\mu$ is the Taylor number, the correction to the Stokes drag force $\mathbf{F}_D$ is, in fact, the time-dependent history force $\mathbf{F}_H$ on the particle [28,29], which is of the order of approximately $T_a^{1/2} 6\pi\mu a\mathbf{v}_s$. In our scheme, $T_a^{1/2}$ is around 0.01, so the rate of approach to the trapping point is modified only slightly by the small history force. As a consequence, the key forces driving this heavy liquid droplet to the stable trapping point are the Stokes drag force from such a vortex and a restoring force $\mathbf{F}_m$ just in the z direction. So the trapping force can be briefly expressed as

$$\mathbf{F}_T = \mathbf{F}_D + \mathbf{F}_m = -6\pi\mu a\mathbf{v}_s - k\mathbf{z}. \tag{2}$$

Hence, a droplet under the stable balance of an external force $\mathbf{F}_{\mathrm{ext}}$ and the trapping force stays stably at one position away from the vortex center. Increasing flow velocity can strengthen the trapping force, so the tweezers are stronger to overcome external interactions. This adjustable trapping force lets the hydrodynamic tweezers have more practical applications.

To further analyze the dynamic process of trapping, we choose the rotating reference frame of angular velocity of $\omega\hat{\mathbf{x}}$, with the origin point at the vortex core, as shown in Fig. 2(b). Then the particle motion equation can be written as

$$\begin{pmatrix}\ddot{y}\\ \ddot{z}\end{pmatrix} = \left(\omega^2 - \frac{k}{2m}\right)\begin{pmatrix}y\\ z\end{pmatrix} + 2\omega\begin{pmatrix}\dot{z}\\ -\dot{y}\end{pmatrix} - \frac{6\pi\mu a}{m}\begin{pmatrix}\dot{y}\\ \dot{z}\end{pmatrix} - \frac{k}{2m}\begin{pmatrix}-\cos(2\omega t) & \sin(2\omega t)\\ \sin(2\omega t) & \cos(2\omega t)\end{pmatrix}\begin{pmatrix}y\\ z\end{pmatrix}. \tag{3}$$

It is noted that now (y, z) is the position of the particle in the rotating frame. The first two terms in the right-hand side (rhs) of Eq. (3) describe the radial motion in a Penning trap [33] shown in Fig. 2(c).

The first term in the rhs of Eq. (3) represents the radial repulsive force $\mathbf{F}_r$ corresponding to the electrostatic potential of a Penning trap, and the second term in the rhs of Eq. (3) represents the Coriolis force corresponding to the Lorentz force of a Penning trap. Without gas damping, the perpetual radial motion of a trapped particle in a Penning trap can be resolved into a fast modified cyclotron motion with angular velocity ω_c' and a slow magnetron motion with angular velocity ω_m. Correspondingly, we have

$$\begin{aligned}\omega_c' &= \omega + \sqrt{\frac{k}{2m}}\\ \omega_m &= \omega - \sqrt{\frac{k}{2m}}.\end{aligned} \tag{4}$$

Now, we consider the buffer gas cooling of a Penning trap [34]. The damping effect refers to the third term in the rhs of Eq. (3). Under the damping effect, the energy of cyclotron motion decreases, and its radius shrinks. But the magnetron motion has a maximum total energy at the center of the trap because of its negative sign of energy. The buffer gas damping causes the particle to move down the magnetron energy hill to a larger radius, which means the failure of trapping the particle at the center. Hence, we need an azimuthal rf quadrupole field in the trap at frequency $2\omega = \omega_c' + \omega_m$ to realize a parametric process that couples the two motions [35]. This is just the last term in the rhs of Eq. (3). The parametric coupling can convert the magnetron motion to the modified cyclotron motion and, combined with the gas damping, causes the magnetron radius also to decrease. Then the particle can be entrapped steadily at the center, as indicated by the trajectories in Figs. 2(b) and 2(c).

Hence, the trapping mechanism of the particle can be understood as a gas damping process of a Penning trap using $(\omega_c' + \omega_m)$ parametric coupling. Then, the condition necessary to achieve trapping is obtained as follows:

$$\omega \le \omega_{\max} = \sqrt{\frac{k_0}{2\rho} + \left(\frac{k_0 a^2}{9\mu}\right)^2}, \tag{5}$$

where $k_0 = 3k/(4\pi a^3)$. When $\omega = \omega_{\max}$, it is the critical condition that the parametric term offsets the damping term

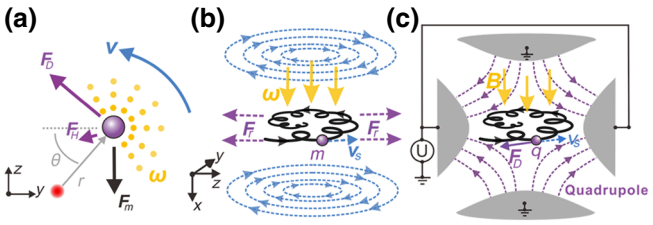

FIG. 2. Trapping dynamics. (a) Force analysis of the droplet in the y-z plane. The red dot indicates the vortex center, and the purple sphere represents the droplet. The angular velocity ω is constant. (b) A sketch of the dynamics of the object in a rotating reference frame. (c) A sketch of the dynamics of the object in a Penning trap with gas damping.

exactly at any moment; then the particle keeps perpetual radial motion as in an ideal classic Penning trap. Turning back to the laboratory reference frame, this critical condition is that the particle travels around the vortex center in a periodic orbit with $\omega = \omega_{\max}$. An angular velocity $\omega < \omega_{\max}$ makes the particle spiral into the trapping center as desired, while a larger ω leads to the escape of the particle.

IV. EXPERIMENTAL MANIPULATION OF THE MICRO-OBJECT

A. Trap

In the experimental realization schematically shown in Fig. 3(a), we employ a microdroplet of water as the target to be controlled by the hydrodynamic tweezers. An array of magnets are used to offset the gravity of the droplet by a diamagnetic effect [36,37]. A tapering glass nozzle is used to generate a particular toroidal vortex in the center region of the magnet array. We use a dosing valve to precisely control the volume flow rate of the gas under an additional pressure P at the inlet. A microscope is used to observe the droplet. Our experiments are carried out at room temperature using nitrogen gas for extensive use. Figures 3(b)–3(d) show the photographs of the setup, the nozzle, and the droplet suspended in the region at the center of magnet array. The region is a cylindrical cavity of radius 0.6 mm and height 1.2 mm. It is noted that the offset force generated by the magnets can be produced by other means, such as by electric forces or dielectric forces, depending on the target material.

To create a droplet in the fluid flow, we use a piezo setup to generate a mist of water with a diameter less than 5 μm. These small droplets spiral into the trapping ring to condense into a bigger one; the trajectories can be seen in Supplemental Video 1 [30]. We control the gas flow velocity at the nozzle outlet by setting the applied pressure P less than 1 psi and tuning the dosing valve precisely. Then we measure the flow velocity to get the ω between $2\pi \times 5$ and $2\pi \times 50$ Hz. At ambient conditions, the viscosity of nitrogen gas is 17.6 μPa s. The droplet is liquid water of density $\rho = 1.0\ \mathrm{g\,cm^{-3}}$ and volume magnetic susceptibility $\chi_v = 9.0 \times 10^{-6}$. During the process of capturing these submicron particles with our hydrodynamic tweezers, we can get control of the droplet size by tuning the time duration of water mist generation. Droplets with diameter ranging from as large as 300 μm to less than 10 μm can be stably trapped. For a smaller droplet (less than 3 μm), trapping becomes unstable and escaping becomes frequent. The reason is that, for a small droplet, the instability of the flow becomes so significant that the drag force pulls the object along the velocity of the fluid and eventually makes it fly out of the bound field as a result of centrifugal force.

The micronozzle used to generate gas flow is made of a glass tube with an inner diameter 1 mm and is fabricated by a heating-pulling process. A nozzle with outlet diameter d being about 20 μm can generate a trapping ring with a radius around 210 μm, which is insensitive to the flow velocity and droplet size. The nozzle is mounted on a manual positioner so that the position of the gas flow field can be tuned.

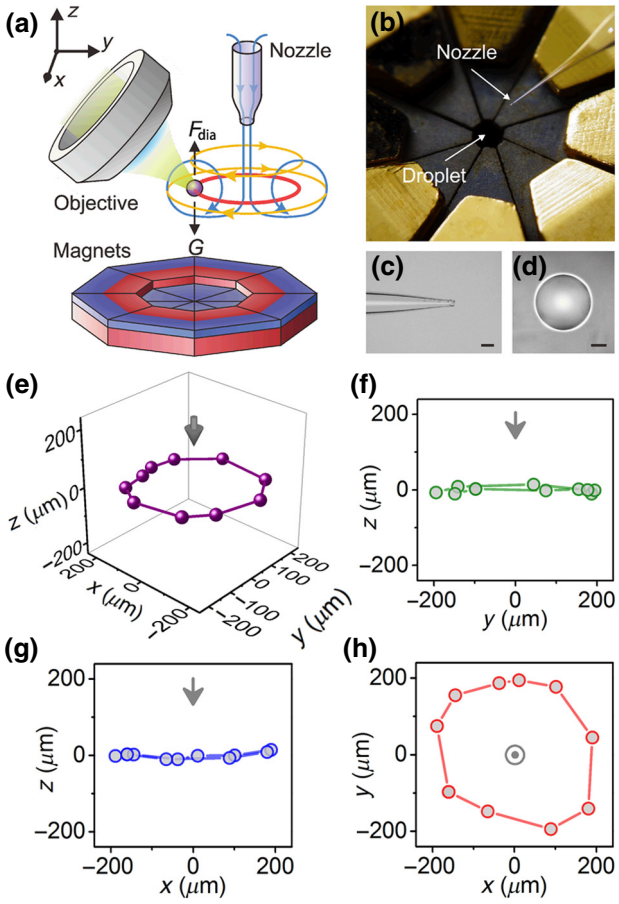

FIG. 3. Experimental trap of a droplet using hydrodynamic tweezers. (a) Schematic plot of the construction of the hydrodynamic tweezers. An array of magnets generates the diamagnetism force to offset the gravity of the droplet; then the vortex field can easily trap the water droplet. A microscope is used to record the position as well as the motion of the droplet. (b) Photograph of the tweezers structure. A microdroplet of droplet can be trapped in the center region of the magnet array. (c) Photograph of the nozzle made from a glass tube with a 1-mm inner diameter. (d) Photograph of a typical microdroplet being trapped. The droplet is spinning, which can be observed in the condensing process (see Supplemental Video 1 [30]). (e) The measured positions of the microdroplet that are obtained by slightly changing the relative location of the magnetic field to the nozzle. The positions clearly show a ring structure as expected; the slight deformation is due to the imperfection of the nozzle and the boundary effect from the center region of the magnet array. The gray arrow indicates the position of the nozzle tip. (f)–(h) The projection of data in (e) to the y-z, x-z, and x-y planes.

We build the diamagnetic trap using an array of 16 pieces of micromachined (Nd, Fe)B permanent magnets of the same structure (see Sec. II of the Supplemental Material [30]), and they are held by a copper unit. The strength of the restoring force near the equilibrium is $k = 4\pi a^3 k_0/3$, with $k_0 = 4.69 \times 10^7$ Nm^{-4}. Theoretically, the droplet is steadily trapped at any position along the trapping ring, but in the presence of the diamagnetism-gravity potential, there is only one trapping point close to the center of the magnetic bound field. The position of the magnets can be slightly tuned to generate an external force $\mathbf{F}_{\text{ext}}$, which can be utilized to pull the droplet. So the equilibrium position of the droplet along the trapping ring can be controlled. Figure 3(e) shows the measured positions where the droplet is trapped by the tweezers. As expected, the stable equilibrium positions only exist on the trapping ring.

B. Transport

Having achieved the trapping of droplet, we continue to test transport behavior of the micro-droplet along trapping ring, the experimental process is shown in Fig. 4(a). A glass needle that works as a disturber is put to be close to the path of droplet. The van der Waals (vdW) interaction between droplet and needle surface is so strong that the droplet will attach to the surface of the needle in the absence of gas flow. For the hydrodynamic tweezers here, however, the droplet is bounded on the trapping ring. So when the external disturber is approaching, besides vdW interaction, there is also hydrodynamic interaction between the droplet and surface. Then the droplet would bypass the disturber.

The fluid flow in the vicinity of the disturber develops boundary layers. In the boundary layer, the velocity of gas flow drops down to zero when approaching the disturber surface. This changes the trapping field regularly. On the other hand, the robustness of the vortex field helps keep its topological structure that remains as a closed loop even when the disturber is approaching. This ensures that the trapping ring also keeps its topological structure.

Numerical simulations affirm that, when the needle comes close from the outer or inner sides of the trapping ring, the ring is always pushed away from the disturber but remains as a closed loop. Figures 4(b)–4(e) plot the numerical simulations of the velocity and the vorticity fields, where the droplet can still be trapped in the ring under the influence of the disturber. As shown in Figs. 4(b) and 4(c) and Figs. 4(d) and 4(e), the vortex field lines together with the trapping ring can always bypass the disturber from the outer and inner sides of the ring, respectively. Figures 4(b) and 4(d) show that the trapping point is always pushed away from the disturber in both situations. From one perspective, the droplet feels a repulsive force from the disturber.

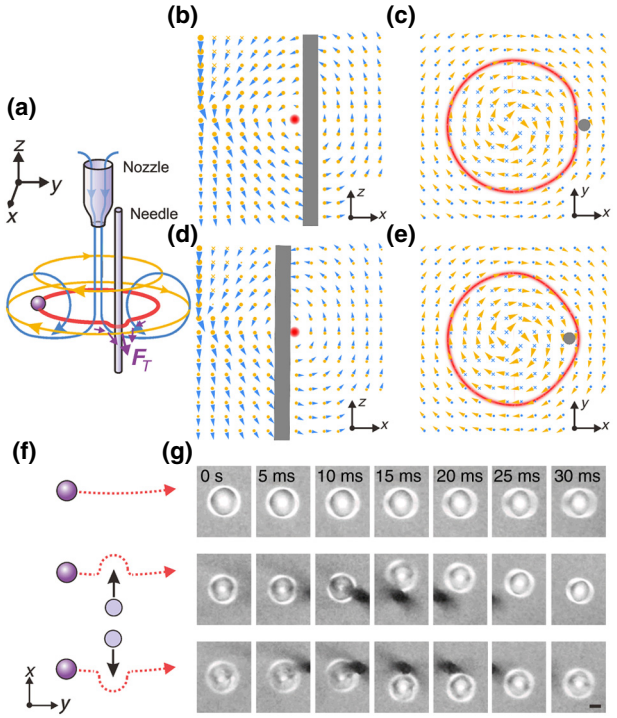

FIG. 4. Self-protected transport in the trapping ring. (a) Schematic plot of the transport. A needle serving as an external disturber is placed into the flow field. The microdroplet moves along the trapping ring and automatically bypasses the needle when encountering it. (b),(c) Numerical simulation of the velocity (blue) and vorticity (yellow) fields in the cross sections in the x-z and x-y planes in (a). The disturber is approaching the trapping ring from the outer side. The size of arrows is proportional to the field strength. The red dot in (b) [red ring in (c)] indicates the trapping point (trapping ring). (d),(e) Same as (b),(c), but with the disturber approaching the trapping ring from the inner side. (f) Scheme of three experimental processes. Top to bottom: Without a needle and with needle coming close from the outer and inner sides of the trapping ring. (g) Time-series photographs of transport processes corresponding to (f), with the scale bar being 20 μm (see Supplemental Videos 4 and 5 [30]).

In order to check the proposed mechanism, an external force $\mathbf{F}_{\text{ext}}$ is generated by tuning the position of the external magnetic field, and a glass needle with diameter 20 μm is used as a disturber. We can pull the droplet along the trapping ring with or without a disturber. When there is no disturber, the droplet can travel along the ring smoothly (see Supplemental Video 2 [30]). When the disturber is approaching in all directions, the droplet trapped in the ring always feels a repulsive force (see Supplemental Video 3 [30]). It is also observed that, no matter where we put the disturber, the droplet always bypasses the needle, as shown in Figs. 4(f) and 4(g) (see Supplemental Videos 4 and 5 [30]). For comparison, a suspended droplet without the presence of gas flow is attracted to the needle (see Supplemental Video 6 [30]). Hence, the hydrodynamic tweezers

protect the droplet from being caught by external objects. Such a protection mechanism is, on one hand, from the overall topological property of the vortex field that cannot be changed by local disturbance and, on the other hand, from the robust reconstruction of the trapping force field that automatically pushes the trapping ring away from the disturber.

C. Transfer

Furthermore, we explore the transfer process of the droplet between two hydrodynamic tweezers. As described above, a trapping ring exists as a closed loop that does not break. So in the presence of the second tweezers, there are only two topologies: one is two independent trapping rings and the other is a single loop that is created by merging two rings. With such topologies, we achieve the transfer of a droplet from one tweezers to the other, as schematically shown in Fig. 5(a). This transfer process is confirmed with the numerical simulation shown in Fig. 5(b). We also perform the experiments, and photographs of the four steps in a typical transfer process are presented in Fig. 5(c) (see also Supplemental Video 7 [30]). After many tries of the transfer processes, we find that the process is not sensitive to the position of the nozzle, the relative angle of the two nozzles, or the size of the trapping ring, which is readily achieved as a character of topology.

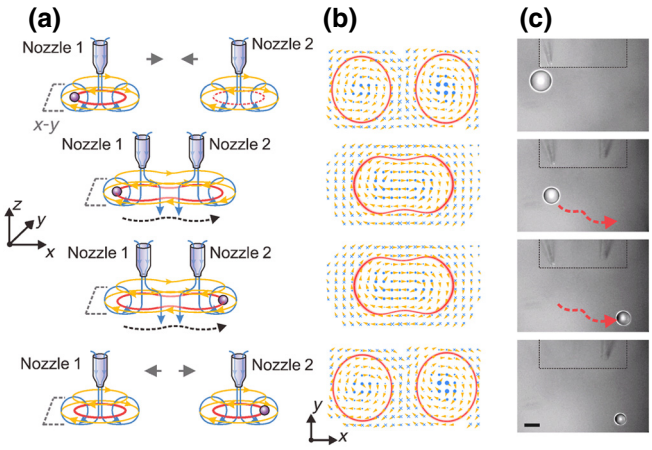

FIG. 5. Topological transfer between two tweezers. (a) Schematic plot of transfer of the droplet from one trapping ring to the other. Top to bottom: The process begins with two tweezers far away from each other and a droplet being trapped in the left one. Then, we move the tweezers close to each other, so that the topological structure of the vortex field is transformed from two separated loops into a single deformed one. Next, we conduct the process of transferring the droplet from left to right using a small external force. Finally, the two nozzles are moved away from each other and the topological structure of the trapping ring returns to the separated case with the droplet being trapped in the right tweezers. (b) Numerical simulations of the velocity (blue) and vorticity (yellow) fields in the cross sections in the x-y plane in (a). (c) Photograph of the droplet in the transfer process described by (a). Inset is the photograph of nozzle tips (see Supplemental Video 7 [30]).

V. CONCLUSION

In summary, we explore and realize a noncontact method to manipulate micro-objects in an easily controllable way. We show that the topological property of fluid flow can be utilized for practical applications. The special character of the hydrodynamic tweezers is that the target object is protected from external disturbances, such as avoiding attaching to a surface. With an adjustable trapping force, the micro-object manipulation techniques demonstrated here are useful in those scenarios where strong interactions are involved, such as scanning microscopy [38] and short-range weak interaction sensing [39,40], as well as a broad range of applications that involve rotation degrees of freedom [41].

ACKNOWLEDGMENTS

We thank Professor Xiaoshun Jiang at Nanjing University for discussions. This work is supported by the National Natural Science Foundation of China (Grants No. 81788101, No. 11675163, and No. 11227901); the National Key Basic Research Program of China (Grant No. 2013CB921800); the CAS (Grants No. QYZDY-SSW-SLH004 and No. GJJSTD20170001); and the Anhui Initiative in Quantum Information Technologies (Grant No. AHY050000).

Peiran Yin and Rui Li contributed equally to this paper and are joint first authors.

[1] A. Ashkin, Acceleration and Trapping of Particles by Radiation Pressure, Phys. Rev. Lett. **24**, 156 (1970).
[2] W. Paul, Electromagnetic traps for charged and neutral particles, Rev. Mod. Phys. **62**, 531 (1990).
[3] D. E. Pritchard, Cooling Neutral Atoms in a Magnetic Trap for Precision Spectroscopy, Phys. Rev. Lett. **51**, 1336 (1983).
[4] P. F. Paradis, F. Babin, and J. M. Gagné, Study of the aerodynamic trap for containerless laser materials processing in microgravity, Rev. Sci. Instrum. **67**, 262 (1996).
[5] A. Nilsson, F. Petersson, H. Jönsson, and T. Laurell, Acoustic control of suspended particles in micro fluidic chips, Lab Chip. **4**, 131 (2004).
[6] I. Bloch, J. Dalibard, and W. Zwerger, Many-body physics with ultracold gases, Rev. Mod. Phys. **80**, 885 (2008).
[7] D. E. Chang, C. A. Regal, S. B. Papp, D. J. Wilson, J. Ye, O. Painter, H. J. Kimble, and P. Zoller, Cavity opto-mechanics using an optically levitated nanosphere, Proc. Nat. Acad. Sci. **107**, 1005 (2010).
[8] I. Tinoco, Jr. and C. Bustamante, The effect of force on thermodynamics and kinetics of single molecule reactions, Biophys. Chem. **101**, 513 (2002).

[9] A. Ashkin, J. M. Dziedzic, and T. Yamane, Optical trapping and manipulation of single cells using infrared laser beams, Nature (London) **330**, 769 (1987).
[10] T. R. Strick, J. F. Allemand, D. Bensimon, A. Bensimon, and V. Croquette, The elasticity of a single supercoiled DNA molecule, Science **271**, 1835 (1996).
[11] C. J. Myers, M. Celebrano, and M. Krishnan, Information storage and retrieval in a single levitating colloidal particle, Nat. Nanotechnol. **10**, 886 (2015).
[12] K. Melde, A. G. Mark, T. Qiu, and P. Fischer, Holograms for acoustics, Nature (London) **537**, 518 (2016).
[13] K. V. Klitzing, G. Dorda, and M. Pepper, New Method for High-accuracy Determination of the Fine-structure Constant Based on Quantized Hall Resistance, Phys. Rev. Lett. **45**, 494 (1980).
[14] M. Z. Hasan and C. L. Kane, Colloquium: Topological insulators, Rev. Mod. Phys. **82**, 3045 (2010).
[15] X. L. Qi and S. C. Zhang, Topological insulators and superconductors, Rev. Mod. Phys. **83**, 1057 (2011).
[16] J. Schaffert, M. C. Cottin, A. Sonntag, H. Karacuban, C. A. Bobisch, N. Lorente, J. P. Gauyacq, and R. Möller, Imaging the dynamics of individually adsorbed molecules, Nat. Mater. **12**, 223 (2013).
[17] M. Hafezi, S. Mittal, J. Fan, A. Migdall, and J. M. Taylor, Imaging topological edge states in silicon photonics, Nat. Photon. **7**, 1001 (2013).
[18] M. C. Rechtsman, J. M. Zeuner, Y. Plotnik, Y. Lumer, D. Podolsky, F. Dreisow, S. Nolte, M. Segev, and A. Szameit, Photonic Floquet topological insulators, Nature (London) **496**, 196 (2013).
[19] S. Mittal, S. Ganeshan, J. Fan, A. Vaezi, and M. Hafezi, Measurement of topological invariants in a 2D photonic system, Nat. Photon. **10**, 180 (2016).
[20] Z. Wang, Y. Chong, J. D. Joannopoulos, and M. Soljačić, Observation of unidirectional backscattering-immune topological electromagnetic states, Nature (London) **461**, 772 (2009).
[21] W. Chen, S. Jiang, X. Chen, B. Zhu, L. Zhou, J. Dong, and C. T. Chan, Experimental realization of photonic topological insulator in a uniaxial metacrystal waveguide, Nat. Commun. **5**, 5782 (2014).
[22] R. Süsstrunk and S. D. Huber, Observation of phononic helical edge states in a mechanical topological insulator, Science **349**, 47 (2015).
[23] X. Wen, C. Qiu, Y. Qi, L. Ye, M. Ke, F. Zhang, and Z. Liu, Acoustic Landau quantization and quantum-Hall-like edge states, Nat. Phys. **15**, 352 (2019).
[24] A. Kitaev, Fault-tolerant quantum computation by anyons, Ann. Phys. (N.Y.) **303**, 2 (2003).
[25] H. K. Moffatt, Experimentally probing topological order and its breakdown through modular matrices, J. Fluid Mech. **35**, 117 (1969).
[26] M. W. Scheeler, W. M. van Rees, H. Kedia, D. Kleckner, and W. T. Irvine, Complete measurement of helicity and its dynamics in vortex tubes, Science **357**, 487 (2017).
[27] T. Gotoh, Brownian motion in a rotating flow, J. Stat. Phys. **59**, 371 (1990).
[28] F. Candelier, Time-dependent force acting on a particle moving arbitrarily in a rotating flow, at small Reynolds and Taylor numbers, J. Fluid Mech. **608**, 319 (2008).
[29] T. Sauma-Pérez, C. G. Johnson, L. Yang, and T. Mullin, An experimental study of the motion of a light sphere in a rotating viscous fluid, J. Fluid Mech. **847**, 119 (2018).
[30] See Supplemental Material at http://link.aps.org/supplemental/10.1103/PhysRevApplied.12.044017 for numerical simulations of fluid flow, design of the magnets, and supplementary videos.
[31] N. A. Chigier and J. M. Beer, Velocity and static-pressure distributions in swirling air jets issuing from annular and divergent nozzles, J. Basic Eng. **86**, 788 (1964).
[32] G. K. Batchelor, *An Introduction to Fluid Dynamics* (Cambridge University Press, Cambridge, 2000).
[33] L. S. Brown and G. Gabrielse, Geonium theory: Physics of a single electron or ion in a Penning trap, Rev. Mod. Phys. **58**, 233 (1986).
[34] G. Savard, St. Becker, G. Bollen, H.-J. Kluge, R. B. Moore, Th. Otto, L. Schweikhard, H. Stolzenberg, and U. Wiess, A new cooling technique for heavy ions in a Penning trap, Phys. Lett. A **158**, 247 (1991).
[35] P. Huang, P. Wang, J. Zhou, Z. Wang, C. Ju, Z. Wang, Y. Shen, C. Duan, and J. Du, Demonstration of Motion Transduction Based on Parametrically Coupled Mechanical Resonators, Phys. Rev. Lett. **110**, 227202 (2013).
[36] M. V. Berry and A. K. Geim, Of flying frogs and levitrons, Eur. J. Phys. **18**, 307 (1997).
[37] A. Winkleman, K. L. Gudiksen, D. Ryan, G. M. Whitesides, D. Greenfield, and M. Prentiss, A magnetic trap for living cells suspended in a paramagnetic buffer, Appl. Phys. Lett. **85**, 2411 (2004).
[38] Y. Nakayama, P. J. Pauzauskiel, A. R. Radenovic, R. M. Onorato, R. J. Saykally, J. Liphardt, and P. Yang, Tunable nanowire nonlinear optical probe, Nature (London) **447**, 1098 (2007).
[39] A. A. Geraci, S. B. Papp, and J. Kitching, Short-range Force Detection Using Optically Cooled Levitated Microspheres, Phys. Rev. Lett. **105**, 101101 (2010).
[40] Q. G. Bailey, V. A. Kostelecky, and R. Xu, Short-range gravity and Lorentz violation, Phys. Rev. D **91**, 022006 (2015).
[41] M. Bhattacharya, Rotational cavity optomechanics, J. Opt. Soc. Am. B **32**, B55 (2015).